Molecular Astrophysics 5 (2016) 1–8

Contents lists available at ScienceDirect

Molecular Astrophysics

journal homepage: www.elsevier.com/locate/molap

Photo-fragmentation behavior of methyl- and methoxy-substituted derivatives of hexa-peri-hexabenzocoronene (HBC) cations

Junfeng Zhen[a,b,*], Pablo Castellanos[a,b], Harold Linnartz[b], Alexander G.G.M. Tielens[a]

[a] Leiden Observatory, Leiden University, P.O. Box 9513, NL 2300 RA Leiden, The Netherlands
[b] Sackler Laboratory for Astrophysics, Leiden Observatory, Leiden University, P.O. Box 9513, NL 2300 RA Leiden, The Netherlands

ARTICLE INFO

Article history:
Received 7 January 2016
Revised 5 August 2016
Accepted 5 August 2016
Available online 10 August 2016

Keywords:
Astrochemistry
PAH cations
Isomerization process
Aromatic
Quadrupole ion trap

ABSTRACT

A systematic study, using ion trap time-of-flight mass spectrometry, is presented for the photo-fragmentation of methyl- and methoxy-substituted derivatives of HBC cations, $(OCH_3)_6HBC^+$ and $(CH_3)_4(OCH_3)_2HBC^+$. Both substituted HBC cations fragment through sequential loss of CH_3CO units upon laser (595nm) irradiation, resulting in a PAH-like derivative $C_{36}H_{12}^+$ and a methyl-substituted PAH derivative $C_{44}H_{24}^+$, respectively. Upon ongoing irradiation, these species further fragment. For lower laser energy $C_{44}H_{24}^+$ dehydrogenates and photo-fragments through CH_3 and $CHCH_2$ unit losses; for higher laser energy isomerization takes place, yielding a regular PAH-like configuration, and both stepwise dehydrogenation and C_2/C_2H_2 loss pathways are found. $C_{36}H_{12}^+$ follows largely this latter fragmentation scheme upon irradiation.

It is concluded that the photo-dissociation mechanism of the substituted PAH cations studied here is site selective in the substituted subunit. This work also shows experimental evidence that photo-fragmentation of substituted PAHs may contribute to the formation in space of smaller species that are normally considered to form by merging atoms and molecules.

1. Introduction

Large polycyclic aromatic hydrocarbons (PAHs) are an important component of the interstellar medium (Tielens, 2008). Their vibrational signatures dominate the mid-infrared spectra of most objects in space and they are key contributors to the energy and ionization balance of the gas. These PAHs are thought to form in stellar ejecta. Subsequently these molecules are further processed for some hundred million years in the harsh environment of the interstellar medium. As part of this evolution, PAHs may acquire functional groups such as methyl, methoxy, and hydroxyl groups (Bernstein et al., 2002). Driven by this astrophysical interest, experiments focusing on the photo-excitation of PAHs have attracted much interest in recent years. A number of different processes can take place, varying from sequential fragmentation and isomerization to ongoing ionization (Cherchneff, 2011; Dunbar, 2000; Ekern et al., 1998; Joblin, 2003; Zhen et al., 2015). Studies of the involved loss channels provide information on the molecular dynamics at play and this is interesting, both from an astronomical and chemical point of view. In photon dominated regions in space, (large) PAHs are considered starting points in the formation of other species, including fullerenes, carbon cages and smaller hydrocarbon chains (Pety et al., 2005). Chemically, the resulting fragments reflect the ongoing dynamics in PAHs upon photon excitation (Berné and Tielens, 2012; Zhen et al., 2014b).

In the optical region, the mechanism proposed to support these processes involves multiple sequential photon absorptions, increasing stepwise the PAH cation internal energy until a dissociation limit is reached, after which fragmentation and isomerization take place (Berné et al., 2015; Montillaud et al., 2013; Walsh, 2008). For vacuum UV wavelengths, ionization and fragmentation compete (Zhen et al., 2015). The majority of these studies has been focussing on 'pure' PAHs. Today, little information is available how photolysis affects substituted derivatives of PAH cations (Jochims et al., 1999; Rapacioli et al., 2015). Such species contain highly active reaction centers that will affect the photo-dissociation efficiency and photo-isomerization process (Bernstein et al., 2002; Lifshitz, 1997; Walsh, 2008). That is, PAH fragments may be more abundant in the interstellar medium than predicted from regular gas phase formation schemes.

In order to characterize the effect of site-substitution on photo-stability and reactivity behavior of PAHs, we present a systematic study of methoxy- and methyl-methoxy-substituted

* Corresponding author.
E-mail addresses: zhen@strw.leidenuniv.nl (J. Zhen), pablo@strw.leidenuniv.nl (P. Castellanos), linnartz@strw.leidenuniv.nl (H. Linnartz), tielens@strw.leidenuniv.nl (A.G.G.M. Tielens).

http://dx.doi.org/10.1016/j.molap.2016.08.001
2405-6758/

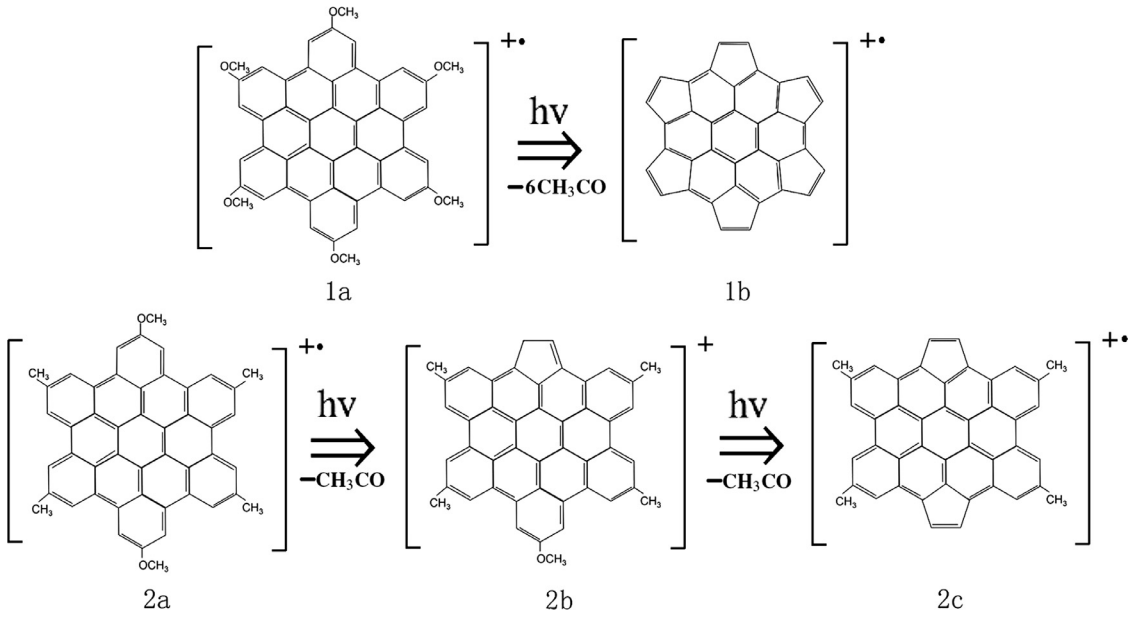

Fig. 1. The molecular geometry, photo-fragmentation products and photo-fragmentation pathway of methoxy- and methyl/methoxy-substituted HBC cation derivatives: the precursor species are 1a $(OCH_3)_6HBC^+$ and 2a $(CH_3)_4(OCH_3)_2HBC^+$.

derivatives of HBC cations, $(OCH_3)_6HBC^+$ and $(CH_3)_4(OCH_3)_2HBC^+$, using quadrupole ion trap time-of-flight (QIT-TOF) mass spectrometry. With 42 C-atoms and 18 H-atoms, HBC is a large PAH; its photo-fragmentation behavior has been studied in detail before by Zhen et al. (2014a). It therefore is possible to compare the data obtained here for the site-substituted HBC cations with those reported earlier for pure HBC cations.

2. Experimental methods

We have studied the photo-fragmentation processes of methoxy- and methyl-methoxy- substituted HBC cations in the laboratory using a quadrupole ion trap (QIT) time-of-flight (TOF) system, i-PoP, our instrument for Photodissociation of PAHs, which has been described in detail in Zhen et al. (2014a). Here only the relevant details are provided. The neutral precursor samples are non-commercial, and transfered into the gas phase by heating powder (purity higher than 95%) in an oven until it slowly starts evaporating; the temperature of the oven is around 630K. Subsequently, the evaporated molecules are ionized by an electron gun and transported into the ion trap via an ion gate. He buffer gas is introduced continuously into the trap for collisional cooling. The working pressures in QIT and TOF chamber are $\sim 3.0 \times 10^{-7}$ and $\sim 3.0 \times 10^{-8}$ mbar, respectively. The light source to irradiate the trapped ions is a tunable dye laser (LIOP-TEC, Quasar2-VN) pumped by a Nd:YAG laser (DCR3, SpectraPhysics), operated at 10Hz. The output of the pulsed dye laser (linewidth ~ 0.2 cm^{-1}, pulse duration ~ 5 ns) is guided horizontally through the ion trap. Experiments are performed at 595 nm. The laser intensity can be varied and is measured by a power meter (Vector, H310) before the laser beam enters the vacuum chamber. A stored waveform inverse Fourier transform excitation (SWIFT) technique (Doroshenko and Cotter, 1996) is used to isolate the precursor (or resulting fragment) ions further allaying any concerns on the sample purity. This substantially improves the quality of our data, as will be shown later. The hardware for the SWIFT setup comprises an arbitrary waveform generator (AWG) board (PCI-5412, NI) that is connected to the ion trap entrance end cap. To synchronize the SWIFT isolation signal with the experimental sequence of i-PoP, the excitation gating and auxiliary digital signals are decoded and reconfigured to allow the insertion of the SWIFT isolation signal.

i - PoP operates at a typical frequency of 0.2Hz. A high precision delay generator (SRS DG535) controls the full timing sequence. Each scan cycle begins with an empty ion trap. At the leading edge of the master trigger the ion gate opens, allowing the ion trap to fill for a certain amount of time with ions that are continuously generated by evaporation and subsequently ionized through electron impact. Once the ions are trapped, the SWIFT technique is applied to isolate a specific range of mass/charge (m/z) species. After a short time delay (typically $\sim$ 0.2s), the ion cloud thermalizes to room temperature ($\sim$ 298K) by collisions with the He buffer gas. The beam shutter opens and the ion cloud is irradiated by light pulses of the dye laser. At the end of the irradiation, a negative square pulse is applied to the end cap, accelerating the ions out of the trap and into the field free TOF region where the resulting mass fragments are measured. A LABVIEW program automates the full data acquisition process.

3. Results

The methoxy- and methyl-methoxy-substituted HBC cation derivatives studied here are shown in Fig. 1. The methoxy precursor (geometry 1a; $(OCH_3)_6HBC$) has a m/z of $^{12}C_{48}\ ^{16}O_6H_{30}^+ = 702.2$, and the methyl/methoxy precursor (geometry 2a, $(CH_3)_4(OCH_3)_2HBC$) has a m/z of $^{12}C_{48}\ ^{16}O_2H_{30}^+ = 638.2$.

Fig. 2 shows the mass spectrum of the trapped methoxy HBC cations substitute (geometry 1a), which contains six OCH_3-units. The top mass spectrum is obtained without laser irradiation and SWIFT signal isolation, and illustrates that the parent cations experience substantial fragmentation due to the electron impact ionization and fragmentation. The improvement in mass purity becomes clear from the lower two panels, where mass peaks at m/z=702.2 for the precursor species (geometry 1a) and at 444.1 for a photo fragment (geometry 1b) are shown using the SWIFT pulse isolation. This also shows that the relatively small isotopic contributions from ^{13}C or ^{18}O, at m/z = 703.2 & 704.2 are suppressed effectively by the SWIFT pulse.

Fig. 3A and (B) show the mass spectra of these selected cations when irradiated by 595 nm photons. Fig. 3A compares the mass

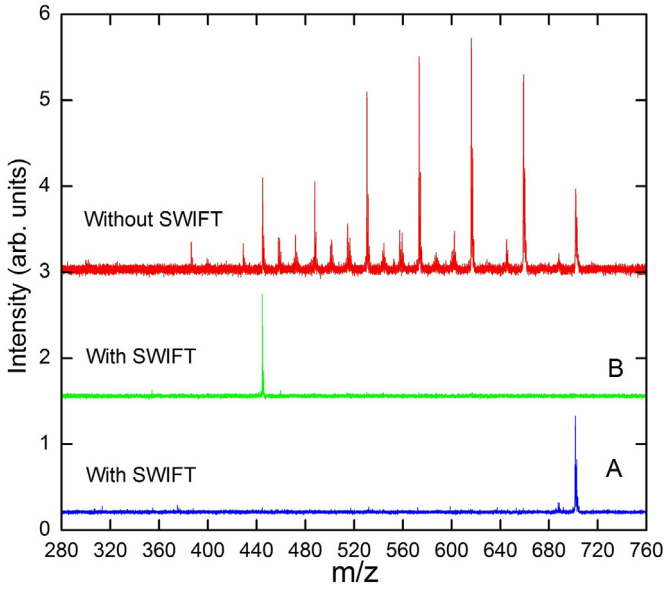

Fig. 2. The mass spectrum of $(OCH_3)_6HBC$ cation, without (red curve) and with (green and blue curve) isolation. Panel A (blue) at mass 702.2 amu corresponds with the isolated precursor cation shown in Fig 1, 1a; panel B (green) at mass 444.1 amu reflects the isolated photo-fragment cation in Fig 1, 1b. (For interpretation of the references to color in this figure legend, the reader is referred to the web version of this article.)

spectra of the trapped precursor species without irradiation (lower panel) and upon 10.5 mJ irradiation (upper panel), illustrating a clear fragmentation behavior upon photo excitation. Mass peaks are found for fragment masses at m/z = 444.1, 487.1, 530.1, 573.1, 616.1, 659.1 and at the precursor mass 702.2, separated by 43Da mass differences. This corresponds to a methoxy-group plus one carbon, suggesting an effective CH_3CO unit (m/z = 43) fragmentation channel. It is not fully clear whether this fragmentation channel involves a single step process, in which an acetyl radical is formed per methoxy side group, or whether the fragmentation takes place through the sequential loss of a CH_3 and CO unit (see Section 4). To further characterize this, also the fragmentation pattern upon electron impact ionization is discussed.

In Fig. 4, we show the mass spectra of geometry 1a with electron impact ionization and fragmentation in different mass ranges, from top panel to down panel, these are as P-43∗(n-1) to P-43∗n, P=702.2 and n=[1, 6], respectively. The vertical lines marked in the figure correspond to peaks with mass differences of 16Da, 30Da and 43Da. As we can see, beside the CH_3CO unit loss channel (43Da), the mass spectra shown in Fig. 4 reveal the presence of several – possibly minor – loss channels involving loss of H, $CH_{2/3}$ (m/z = 14/15), O (m/z = 16) and $OCH_{1/2}$ (m/z = 29/30) fragments (see Section 4where this is further discussed). These minor channels are not visible in the photo-fragmentation results (Fig. 3A), possibly because intermediary products are limited in intensity. In either case, photo irradiation or electron impact, in the end, a carbon atom is extracted from the HBC backbone structure resulting in the formation of a pentagon structure is indicated.

After the sequential loss of all six CH_3CO units, a ring structure with six pentagons remains as shown in Fig. 1 (geometry 1b). Fig. 3B shows the resulting mass spectrum of this fragment upon 595 nm irradiation for different laser intensities, again before (upper panel) and after irradiation (other panels). It is found that this m/z = 444.1 fragment dehydrogenates, mainly through sequential 2H (or H_2) losses, leading to the predominance of even-mass species $C_{36}H_{12-2*n}{}^+$ with n = [0 − 6]. Ultimately, the parent ion loses all its 12 hydrogen atoms, ending at m/z = 432, a bare carbon cluster containing 36 C-atoms. Fig. 3B also shows that the degree of dissociation depends on the incident radiation flux; with increasing power, fragmentations of the carbon skeleton become more prominent. Masses corresponding to $C_{36-2*n}{}^+$, n= [0 − 3] appear reflecting sequential C_2 or C_2H_2 losses, as we also observe low concentrations of intermediates hydrogenated fragments. In summary, after loss of the methoxy groups, dehydrogenation and C_2 or C_2H_2 loss channels dominate the fragmentation behavior. This is very similar to the photo-fragmentation behavior of pure HBC cations (Zhen et al., 2014a).

Fig. 5 shows the mass spectrum of the other precursor species studied here, an HBC geometry with four methyl- and two methoxy-unit substitutes, $(CH_3)_4(OCH_3)_2HBC^+$. The top spectrum is obtained without laser irradiation and SWIFT signal isolation. Again, the parent cations exhibit a large degree of dissociation due to the electron impact ionization. With a SWIFT pulse pre-set masses can be selected; in panels (A), (B) and (C), this is illustrated for mass trapping at m/z = 638.2, 595.2 and 552.2, respectively.

Fig. 6A (geometry 2a; m/z = 638.2) and 6B (geometry 2b; m/z = 595.2) show the resulting fragmentation pattern of the selected cations upon irradiation with 595 nm photons. In Fig. 6A two main fragments are found with peaks at m/z = 595.1 and 552.2, again separated by a 43Da mass difference. These are clearly absent in the lower panel where no laser light is used. Fig. 6B shows the mass spectrum of geometry 2b (m/z = 595.2), after irradiation, and here one strong fragment shows up at m/z = 552.2 without further fragmentation. Also these two peaks are separated by a 43Da mass difference. The interpretation of this observation is the same as in the fully methoxy-substituted derivative, i.e., that photo-fragmentation is governed first by the sequential loss of the two CH_3CO units. It is interesting to note that this channel is clearly preferred above fragmentation via the loss of a methyl group (see Section 4 where this is further discussed). The dissociation pathway of geometry 2a and the structure of the resulting fragments (geometries 2b and 2c) are shown in Fig. 1. As in the previous case, also for this molecule we discuss the fragmentation behavior upon electron impact ionization.

In Fig. 7, we show the mass spectra of geometry 2a with electron impact ionization and fragmentation in different mass ranges, from top panel to down panel, these are as P-43∗(n-1) to P-43∗n, P = 638.2 and n = [1, 2]. The vertical lines marked in the figure correspond to peaks with difference of 16Da, 30Da and 43Da. As we can see, structure 2a has a similar fragmentation behavior as structure 1a, only the intermediate that is formed by electron impact has a lower intensity. Also, in the electron impact experiment, the CH_3CO unit loss channel is preferred to the methyl unit loss channel.

Fig. 8 shows the fragmentation behavior of geometry 2c, without methoxy but still with all four methyl groups (m/z = 552.2), as function of different laser intensities. Our interpretation of the dissociation pathway of geometry 2c at low laser energy and the likely structure of all fragments is shown in Fig. 9A. The general trend follows dehydrogenation and carbon loss channels, but the full photo-fragmentation pattern is more complex than found for geometry 1b or other PAH cations (Zhen et al., 2014a). The likely explanation for this observation is that geometry 2c not only comprises a carbon skeleton with pure aromatic properties, but in addition contains four reactive CH_3 units. This is also reflected in the laser intensity dependent behavior (Fig. 8). In analogy to fragmentation studies on the toluene cation (Huang and Dunbar, 1991), we surmise that H-loss from a methyl group initiates isomerization to a tropylium structure (see Section 4). Additionally, we see evidence for carbon loss channels separated by 15Da and 27Da mass differences, which suggests two independent dissociation pathways: one is via CH_3 loss, the other through loss of a C_2H_3 unit, resulting in a five carbon ring structure (c.f., Fig. 9A). Likely, the latter involves

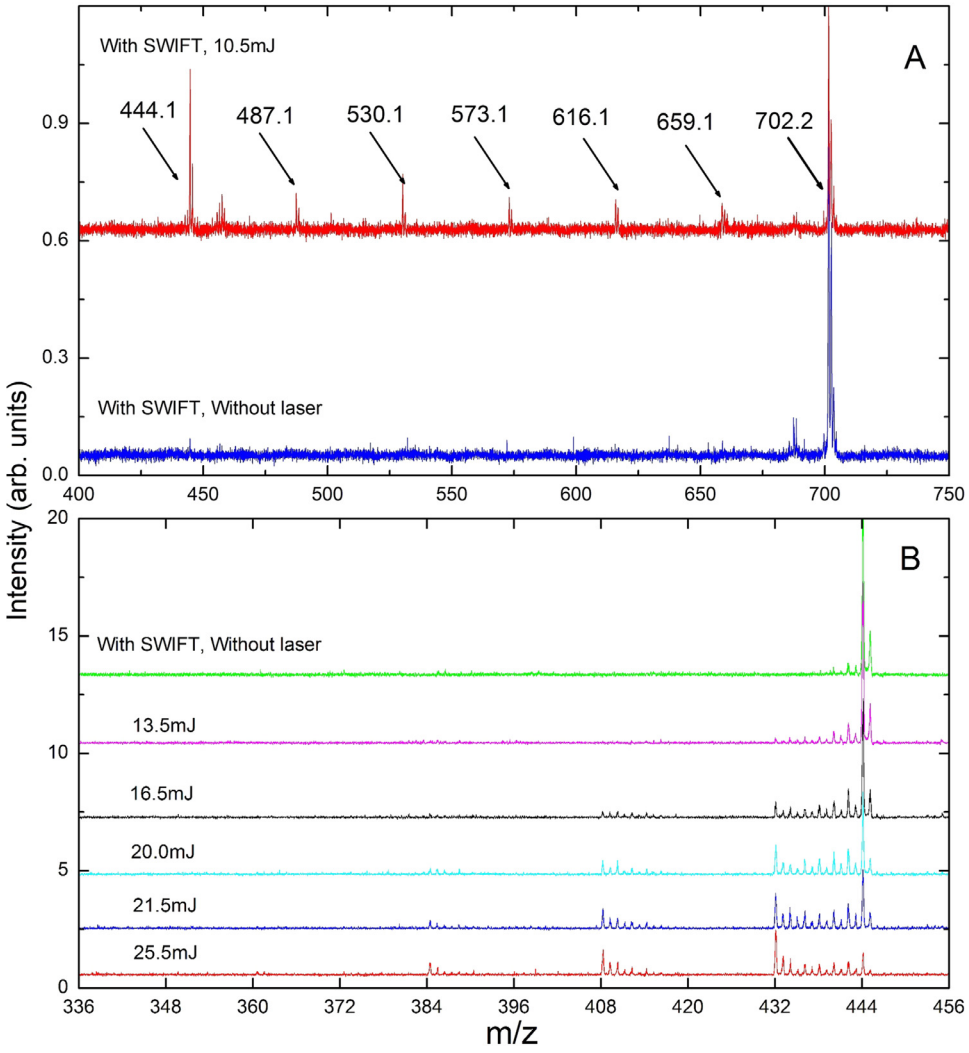

Fig. 3. Panel (A): Mass-spectrum of geometry 1a (lower graph) and the mass spectrum with irradiation at 595 nm. Panel (B): Mass-spectrum of geometry 1b, before (upper panel) and with irradiation at 595 nm at different laser powers.

isomerization to a vinyl $CHCH_2$ group but our experiments are not allowed to directly address this issue. The corresponding process is shown in Fig. 9 as well.

The dissociation pathway of geometry 2c at high laser fluences is different and our interpretation of the results is summarized in Fig. 9B. For higher laser energy – e.g., at 12.5mJ –, m/z = 456, 480, 504 and 528 peaks appear with 24Da mass differences; 24Da corresponds to a loss of two C-atoms (C_2 m/z = 24). The mass peaks are therefore assigned as m/z = 456, C_{38}^+; 480, C_{40}^+; 504, C_{42}^+ and 528, C_{44}^+. These observations are consistent with structural rearrangements. After the cumulative loss of 4 H-atoms from the four individual CH_3 units, the benzyl ion structure will possibly transfer into a tropylium ion structure, changing to a geometry with aromatic properties (Ausloos, 1982). After that, dehydrogenation and C_2/C_2H_2 loss pathways will dominate the photo-fragmentation. At that point, the fragmentation behavior follows that previously observed for the HBC cation, where the different photo-fragmentation efficiencies depend directly on the incident radiation flux (Zhen et al., 2014a).

4. Discussion and astrophysical relevance

The fragmentation behavior of methoxy substituted HBC cations is akin to that of substituted benzene and small PAHs. Fragmentation of anisole reveals two pathways: (1) Formaldehyde loss followed by H loss resulting in phenyl, (2) Methyl loss followed by CO loss, leading to cyclopentadienyl formation (Mohan, 2003). Fragmentation of methoxy-PAHs has been studied upon electron impact (Barnes et al., 1967). For naphthalene substituted at the α site, fragmentation leads to pentagon formation in a two step process (CH_3 loss followed by CO loss) with no evidence for the formaldehyde loss channel (Barnes et al., 1967). Fragmentation of 2-methoxy-naphthalene, on the other hand, does reveal both channels. The 1-, 2-, 3-, 4-methoxy-phenanthrenes follow the two-step pathway of 1-methoxy-naphthalene with no significant loss of formaldehyde. In these electron impact experiments, the importance of the two step process is invariably revealed by a clear peak at the intermediate mass (parent−15). However, fragmentation of 9-methoxy-phenanthrene is unique as it shows clear evidence for an one-step process of elimination of a CH_3CO unit – likely in the form of a acetyl radical – and it has been suggested that this is connected to the stability of the fluorenyl ion (Barnes et al., 1967). The electron impact studies show that dimethoxy-phenanthrene and -naphthalene lead to formation of two pentagons as the fragmentation pathways for these PAHs (Barnes et al., 1967).

As discussed in Section 3, in our experiments, we see that electron impact can proceed through a one-step process, but a (even) dominant contribution from a two-step process cannot be

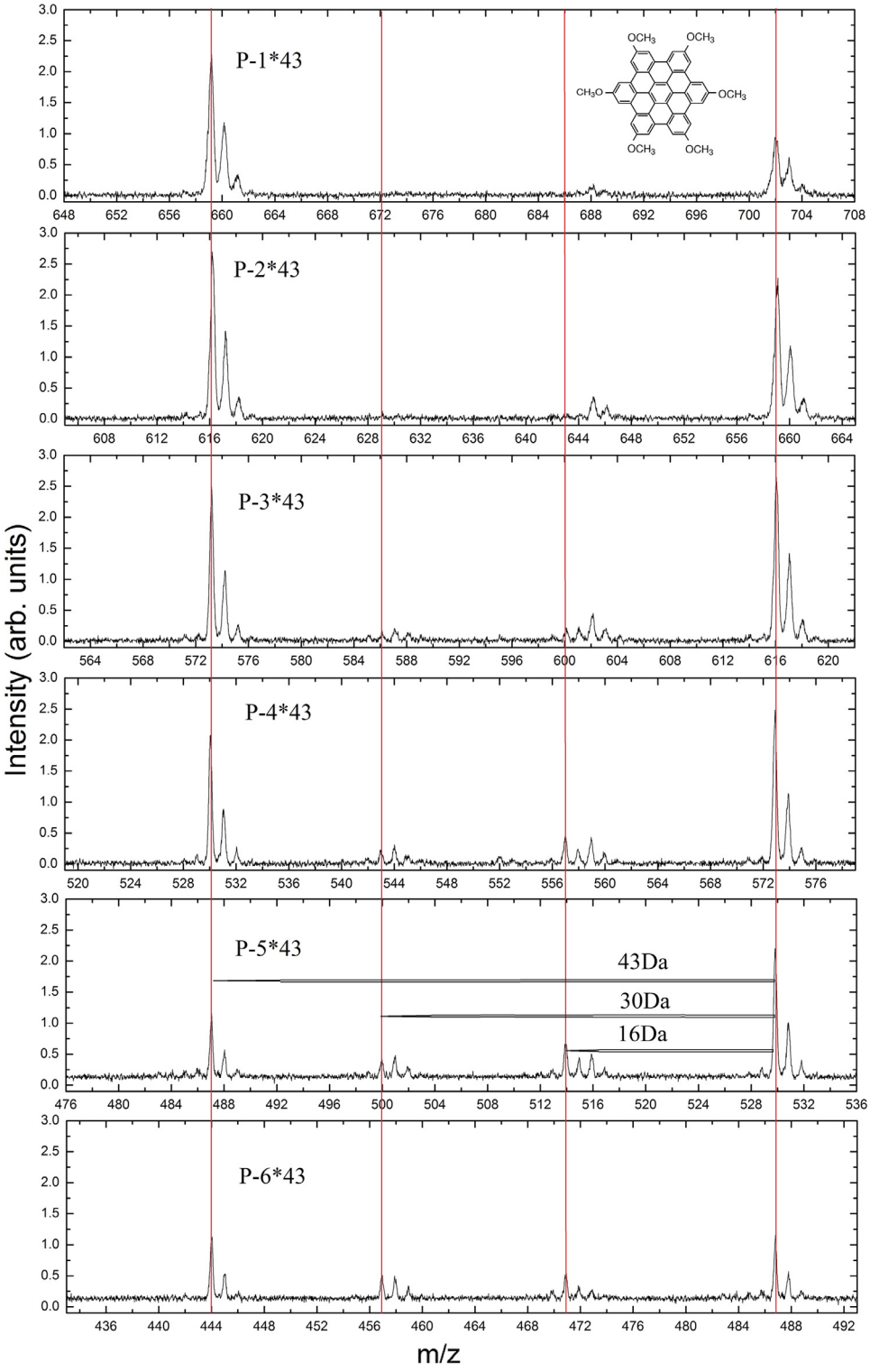

Fig. 4. The mass spectrum of $(OCH_3)_6HBC$ natural molecules with electron ionization and fragmentation, before isolation, in different mass ranges. The different panels are partially overlapping and shown in such a way that 43Da mass losses overlap (in between the left and right vertical line). The two remaining lines indicate 30 and 16Da mass differences.

excluded. Our photo experiments reveal that photons are efficient in removing the methoxy; the methoxy-group removal runs quickly to completion and intermediate steps in the sequential removal of CH_3CO units loss are very weak. Our electron impact and photo experiments do demonstrate, though, that this process of methoxy group removal can be continued all the way to completion and the formation of six pentagons.

Fragmentation of methoxy- and methyl-substituted phenanthrene has been studied by electron impact (Barnes et al., 1967). As for the methoxy- and methyl-substituted HBC cations in this study, fragmentation of 3,6 dimethoxy -9,10-dimethyl phenanthrene is dominated by the oxygen function in a two step process with a passive role for the methyl groups. Thermal decomposition studies in shocktube experiments have yielded Arrhenius energies for the

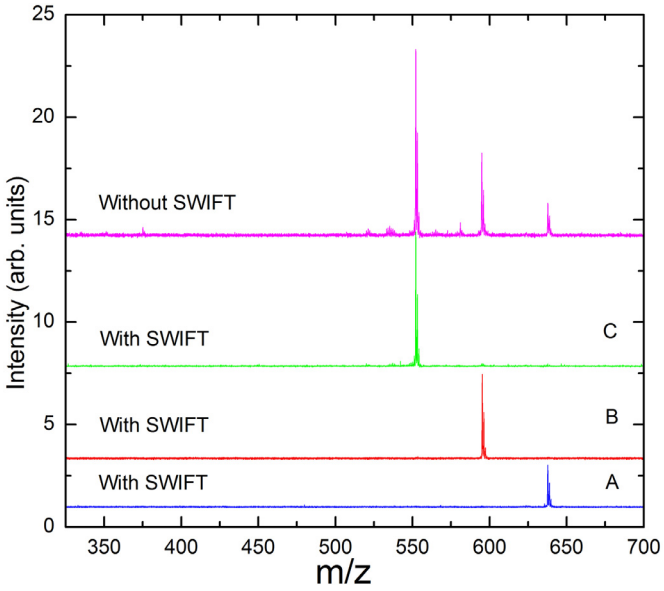

Fig. 5. The mass spectrum of $(CH_3)_4(OCH_3)_2$HBC cation, without (magenta curve) and with (green, red and blue curve) isolation. Panel A (blue) at mass 638.2 amu corresponds with the isolated cation shown in Fig. 1, 2a; Panel B (red) at mass 595.2 amu corresponds with the isolated cation shown in Fig. 1, 2b; Panel C (green) at mass 552.2 amu corresponds with the isolated cation shown in Fig 5, 2c. (For interpretation of the references to color in this figure legend, the reader is referred to the web version of this article.)

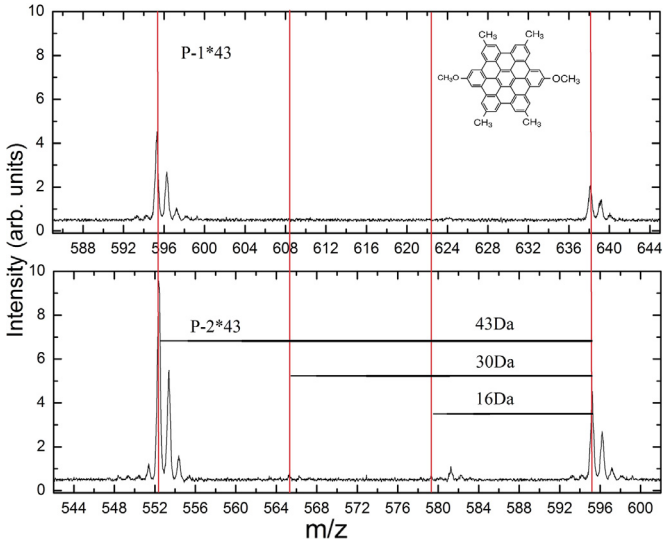

Fig. 7. The mass spectrum of $(CH_3)_4(OCH_3)_2$HBC natural molecules with electron ionization and fragmentation, before isolation, in different mass ranges.

two sequential steps of methyl and carbon monoxide fragmentation of 2.8 and 1.9 eV (Lin and Lin, 1986; Walsh, 2008). We note that the direct channel of acetyl elimination can be competitive in these types of experiments and must have a similar low Arrhenius energy. These Arrhenius energies are readily achievable with our system and are considerably less than involved in H-loss from the methyl group (3.8 eV), methyl group loss (4.5 eV), and aromatic H-loss (4.9 eV). In view of this, we are not surprised that loss of methoxy dominates over methyl group loss in our electron impact and photo experiments.

Turning now to the fragmentation behavior involving the methyl groups after methoxy elimination, we note that photo fragmentation studies on toluene ions have shown that at low excitation energies (2–3. 5eV), H-loss initiates with the isomerization to the tropylium structure and only at higher energies does fragmentation to the benzyl structure become competitive (Huang and Dunbar, 1991). DFT calculations show that the pyrenemethylium cation ($[C_{16}H_9\text{-}CH_2]^+$) is slightly less stable (~ 0.1 eV) than the isomer with a heptagon cycle and the free energy barrier between the two isomers is calculated to be 3.5–4 eV (Rapacioli et al., 2015). For comparison, the bond energy of an aromatic hydrogen as well as the hydrogen in a methylene group is 4.47 eV. Hence, as we see complete H stripping taking place, this isomerization process is certainly feasible in our experiments. We note that the methylene group is bonded by 4.9 eV in phenyl. Hence, in either case, we surmise that full H stripping is possible. Our photo experiments consist of multiple steps of photon absorption followed by fragmentation. This sequential processing will favor fragmentation through the lowest energy channels available. Indeed, the fragmentation behavior in our photo experiments – starting with methoxy loss, followed by clear completion between H-loss from the methyl group, H-loss from the methylene group,

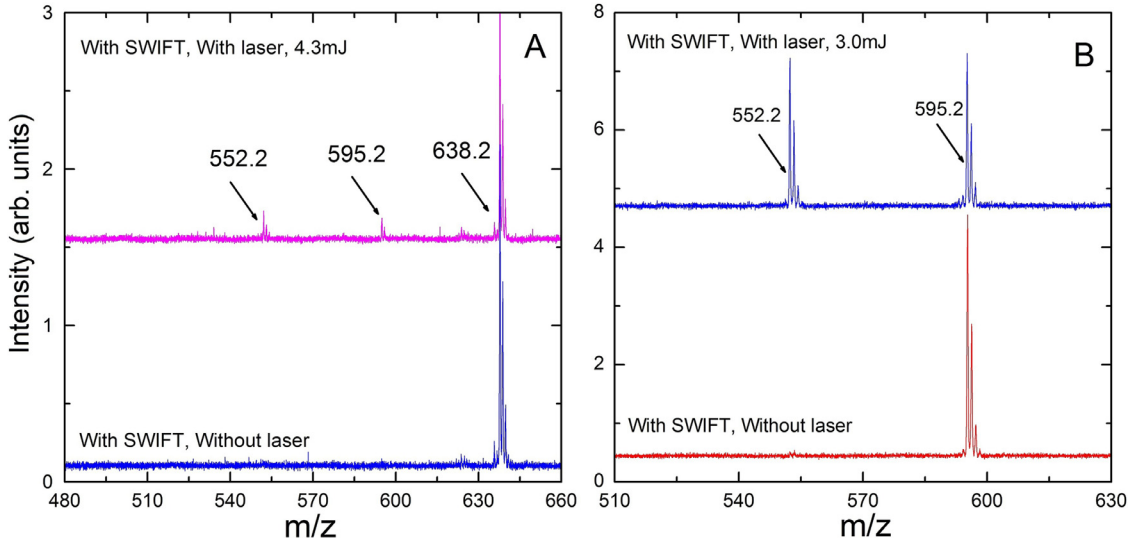

Fig. 6. Panel (A): Mass-spectrum of geometry 2a before and after irradiation with 595 nm. panel (B): Mass-spectrum of geometry 2b before and after irradiation with 595nm.

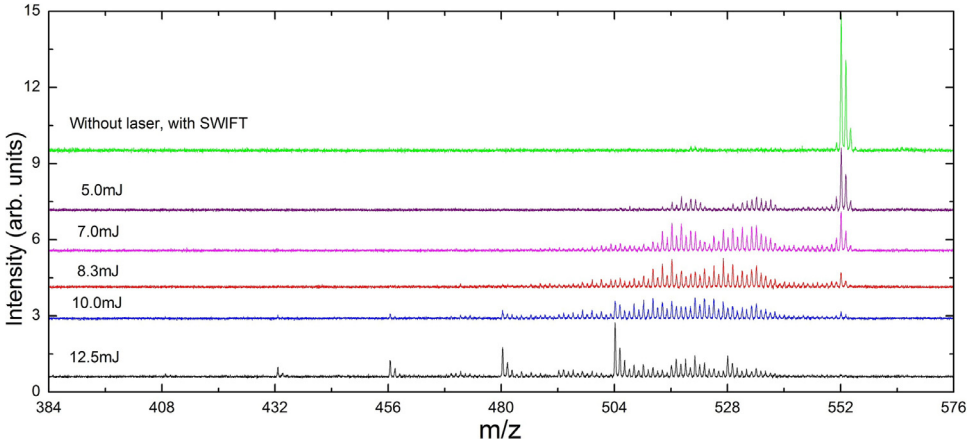

Fig. 8. Mass-spectrum of geometry 2c before and after irradiation with 595 nm for different laser powers.

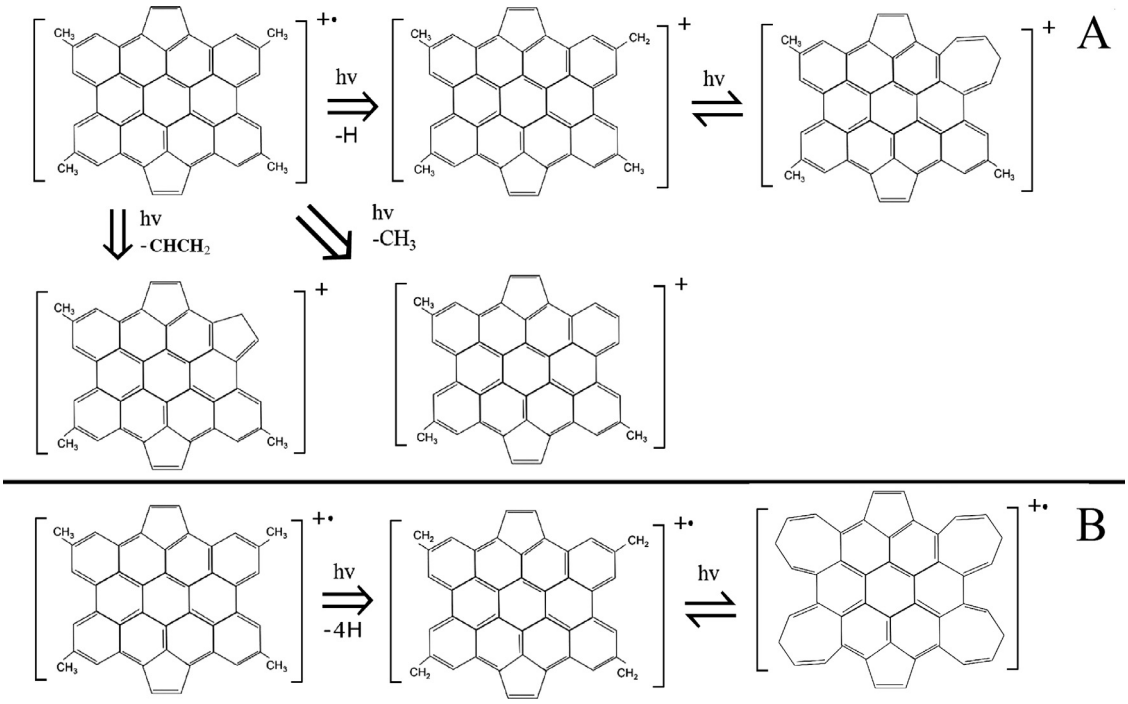

Fig. 9. The geometry, photo-fragmentation products and photo-fragmentation/isomerization pathways of geometry 2c upon 595 nm irradiation. Panel (A): geometry 2c for lower laser energy; Panel (B): idem for higher laser energy.

and aromatic hydrogen loss and then followed by C_2 loss – illustrates the predominance of lowest energy channel well. Hence, we suggest that HBC transforms to a tropylium ion structure with aromatic properties and this pathway is shown in the upper panel of Fig. 9A. In the end, irrespective whether the pathway leads through methylene or heptagon structures, we consider the predominance of the bare carbon clusters at C_{44}, C_{42}, C_{36} evidence for sequential C_2 loss – after all H's are lost – starting from the structure containing the two pentagons and four heptagons shown as the final molecular structure in Fig. 9B.

The study reported here has implications for the photolytic evolution of large PAH molecules in space and their contribution to the presence of small hydrocarbon species. Large PAH molecules are thought to be formed in processes akin to soot formation in the cooling ejecta of carbon-rich red Giant stars as they flow from the stellar photosphere into the interstellar medium of the Milky Way (Cherchneff et al., 1992; Frenklach and Feigelson, 1989). In the interstellar medium, these species are further processed (Tielens, 2008). Inside molecular clouds, PAHs may become trapped in low temperature (10 K) ice mantles, consisting mainly of H_2O with traces of CH_3OH, CO_2, CO, and NH_3 at the 10% level. Photolysis of these complex ice mixtures is known to functionalize these PAHs with alcohol (−OH) and ketone (> C=O), amino ($-NH_2$), methyl ($-CH_3$), methoxy ($-OCH_3$), cyano/isocyano (−CN, −NC), and acid (−COOH) groups (Bernstein et al., 2002). This complex chemistry may be at the basis of the aromatics bearing carbon and nitrogen containing side groups as isolated from primitive carbonaceous meteorites and interplanetary dust particles (Clemett et al., 1993; Sephton, 2002). Moreover, upon heating of these ice mantles in regions of star and planet formation, the functionalized PAHs evaporate with the ice and are then thought to be further processed by abundant UV photons from nearby luminous stars. This so-called top-down chemistry (Berné and Tielens, 2012) may be responsible for the abundant presence of small hydrocarbon radicals in such regions (Pety et al., 2005). Early studies have analyzed the photolytic behavior of functionalized PAHs based upon molecular bond

energies (Geballe et al., 1989), but as the results reported here demonstrate, this has to be reevaluated. Specifically, the chemical routes involved are very product specific and can lead to methyl-group formation but not e.g., formaldehyde or methanol. Further experiments are required on a broader range of functional groups to assess whether this can be utilized to quantitatively probe the contribution of these chemical routes towards the complexity of regions illuminated by strong stellar radiation fields in space.

Finally, we want to emphasize that the results reported here also have implications for the photochemical production of fullerenes and cages from large PAHs (Berné and Tielens, 2012; Zhen et al., 2014b). Laboratory studies have shown that UV photolysis of large PAHs will first strip off all H's, converting these species into small graphene flakes. Further UV processing of these graphene flakes leads then to the formation of cages and fullerenes (Zhen et al., 2014b). This "isomerization" process is inferred to be initiated by C-loss and the formation of pentagons which drive the curling up of the molecular structure into cages. Likely, the efficiency of this process is directly linked to the efficiency of pentagon formation. As this study shows, pentagon formation may be a natural sideproduct of the photolysis of functionalized PAH species and this may be a key step in fullerene formation in the interstellar medium. Further studies will be needed to quantify this route.

Acknowledgments

We are grateful to L. J. Allamandola who provided the samples. Studies of interstellar chemistry at Leiden Observatory are supported through advanced-ERC grant 246976 from the European Research Council, and by the Dutch Science Foundation, NWO, through the Dutch Astrochemistry Network, through a Spinoza premie, and through a NWO VICI grant.

References

Ausloos, P. 1982, J. Am. Chem. Soc., 104, 5259–5265.
Barnes, C.S., Collins, D.J., Hobbs, J.J., Mortimer, P.I., & Sasse, W.H.F. 1967, Aust. J. Chem., 20, 699–712.
Berné, O., Montillaud, J., & Joblin, C. 2015, Astron. Astrophys., 577, A133.
Berné, O. & Tielens, A.G.G.M. 2012, Proc. Natl. Acad. Sci., USA, 109, 401–406.
Bernstein, M.P., Elsila, J.E., Dworkin, J.P., Sandford, S.A., Allamandola, L.J., & Zare, R.N. 2002, Astrophys. J., 576, 1115–1120.
Cherchneff, I. 2011, EAS Publ. Ser., 46, 177–189.
Cherchneff, I., Barker, J.R., & Tielens, A.G.G.M. 1992, Astrophys. J., 401, 269–287.
Clemett, S., Maechling, C., Zare, R., Swan, P., & Walker, R. 1993, Science, 262, 721.
Doroshenko, M.V. & Cotter, R.J. 1996, Rapid Commun. Mass Spectrum., 10, 65–73.
Dunbar, R.C. 2000, Int.J. Mass Spectrom., 200, 571–589.
Ekern, S.P., Marshall, A.G., Szczepanski, J., & Vala, M. 1998, J. Phys. Chem. A, 102, 3498–3504.
Frenklach, M. & Feigelson, E.D. 1989, Astrophys. J., 341, 372–384.
Geballe, T., Tielens, A.G.G.M., Allamandola, L.J., Moorhouse, A., & Brand, P.W.J.L. 1989, Astrophys. J., 341, 278–287.
Huang, F.S. & Dunbar, R.C. 1991, Int. J. Mass Spectrom. Ion Processes, 109, 151–170.
Joblin, C. 2003, ed. Combes, InF, D. Barret, T. Contini, & L. Pagani, SF2A-2003 Semaine de lÁstrophysique Francaise 175–179.
Jochims, H.W., Baumgartel, H., & Leach, S. 1999, Astrophys. J., 512, 500–510.
Lifshitz, C. 1997, Int. Rev. Phys. Chem., 16, 113–139.
Lin, C.Y. & Lin, M.C. 1986, J. Phys. Chem., 90, 425–431.
Mohan, J. 2003, Organic Analytical Chemistry, Theory and Practice: (1st ed. Alpha Science International, Ltd.) P323.
Montillaud, J., Joblin, C., & Toublanc, D. 2013, Astron. Astrophys., 552, A15.
Pety, J., Teyssier, D., Fossé, D., et al. 2005, Astron. Astrophys., 435, 885–899.
Rapacioli, M., Simon, A., Marshall, C.C.M., Cuny, J., Kokkin, D., Spiegelman, F., & Joblin, C. 2015, J. Phys. Chem. A, 119, 12845–12854.
Sephton, M.A. 2002, Nat. Prod. Rep., 19, 292–311.
Tielens, A.G.G.M. 2008, Annu. Rev. Astron. Astrophys., 46, 289–337.
Walsh, R. 2008, Chem. Soc. Rev., 37, 686–698.
Zhen, J., Castellanos, P., Paardekooper, D.M., Ligterink, N., Linnartz, H., Nahon, L., Joblin, C., & Tielens, A.G.G.M. 2015, Astrophys. J. Lett., 804, L7.
Zhen, J., Castellanos, P., Paardekooper, D.M., Linnartz, H., & Tielens, A.G.G.M. 2014b, Astrophys. J. Lett., 797, L30.
Zhen, J., Paardekooper, D.M., Candian, A., Linnartz, H., & Tielens, A.G.G.M. 2014a, Chem. Phys. Lett., 592, 211–216.